Influence of electromagnetic field variations on the surface-effect mechanisms of photofield emission

J. T. Lee and W. L. Schaich
Department of Physics and Materials Research Institute, Indiana University, Bloomington, Indiana 47405
(Received 29 February 1988; revised manuscript received 26 April 1988)

By a series of model calculations the effects of various theoretical ingredients on a simple theory of photofield emission yield are illustrated. Only surface-effect mechanisms are retained, but for reasonable parameter choices the predictions can be made to agree with experimental data. The influence of different possible spatial variations for both the potential-energy barrier and the photon field are treated.

OVERVIEW

Photofield emission is a spectroscopy that combines features of both field emission and photoemission in that electrons are ejected from a surface under the joint influence of a strong, static electric field and weak, dynamic radiation fields. It has the advantage over the separate methods of allowing one to study electronic structure for final-state energies between the Fermi level and the unperturbed vacuum level.

A lot of work has been done on excitation mechanisms that may apply. Both theoretical descriptions and experimental evidence exist for a variety of surface and bulk effects. In this paper we shall consider carefully the predictions of one particular class of models in order to clarify what they can describe. We refer to these as jellium models of photofield emission and acknowledge that they have been studied often before with various goals and degrees of sophistication.[1-16] The primary simplification of such models is that they exclude effects due to discrete atoms; in particular, they contain none of the conventional bulk transitions. Hence we will discuss neither the experimental evidence nor the theoretical methods developed for bulk band-structure or band-gap surface states.[17-29] In their favor the jellium models can treat all the pure surface-excitation effects, and their predictions even at the simplest level[3,7] give a reasonable qualitative description of the energy-distribution curves seen experimentally.[30-32] Indeed, a common method of identifying structure due to bulk effects is to compute first the predictions of a (scaled) jellium model and then, by comparison with the experimental data, find the (generally) small deviations.

Our particular interest with jellium models here involves the question of scale and we focus on the absolute value of the yield per incident photon. The data recently published by Gao and Reifenberger[16] for the (110) and (111) faces of W provide the experimental information that we compare with, but one should not expect a jellium model to represent quantitatively the behavior of a transition metal. Our emphasis will be more on understanding the theoretical ingredients of such a calculation and their surface sensitivity. We agree with the conclusion found by Feibelman[33] for regular photoemission that the total yield is much more surface sensitive than are its distribution over energy and angle.

Our theory is based on the independent-particle approximation, but in several places we use quantities which for *a priori* values require many-body calculations. We completely neglect damping effects for the photoelectron and for the hole left behind. We assume both move in a common potential energy $V(x)$, which for a smooth surface depends only on x, the normal coordinate, and which quickly saturates to a constant value in the bulk; see Fig. 1. As an aside, note that the experimental resolution[34] of the puzzle of (static) field-dependent oscillations in the yield argues against the need to include dynamic image-potential effects in V,[10-13,35] and we do not. The radiation field driving the transitions is viewed as acting only through the normal component of its vector potential, $A_x(x)$, since it alone has a significant variation near the surface; see Fig. 1. Our accounting for this variation is the principal new feature of the calculations.

With these basic ingredients the reduction of general photoemission theory is straightforward.[36] The problem becomes essentially one dimensional since the eigenstates of both electrons and photons have factors of plane waves for motion parallel to the surface and since the parallel wave vector of the photon is generally negligible compared to that for the electron. The net result is that A_x alone acts to excite electrons, which transition between eigenstates of motion along x, conserving their wave vectors parallel to the surface. From the golden-rule formula for photoemission, we find that the yield per incident photon in a jellium model can be written as

$$Y=\int dE\, Y(E)\ , \tag{1}$$

where $Y(E)$, the (final) energy distribution of the yield, is

$$Y(E)=\frac{2\alpha}{\pi}\left[\,|t|^2\frac{\sin^2\theta}{\cos\theta}\cos^2\phi_p\right]\frac{f(E-\hbar\omega)}{\hbar\omega} \times\int^E dW_f\frac{1}{(W_iW_f)^{1/2}}T(W_f)\,|M_{fi}|^2\ . \tag{2}$$

Here, $\alpha=e^2/\hbar c$ is the fine-structure constant, $\hbar\omega$ is the photon energy, θ its angle of incidence, and ϕ_p the angle between its polarization vector and the plane of in-

cidence. The factor

$$t=\frac{2\cos\theta}{\epsilon\cos\theta+(\epsilon-\sin^2\theta)^{1/2}} \tag{3}$$

is the Fresnel transmission amplitude for a (p-polarized) wave to refract from vacuum into a metal of dielectric function $\epsilon(\omega)$. An alternate expression for the contents of the square brackets in (2) is

$$[\cdots]=(\cos\theta)^{-1}\,|\,A_x(B)\,|^2/|\,\mathbf{A}(I)\,|^2\,, \tag{4}$$

where $\mathbf{A}(I)$ is the full vector potential of the *incident* photon and $A_x(B)$ is the normal component of the refracted field in the *bulk*. These fields are to be evaluated far from the surface on the scale of electronic screening lengths, but close to the surface on the scale of a transverse wavelength or skin depth. Typically, a few tens of angstroms away from the surface satisfies these constraints; see Fig. 1.

Before describing the rest of (2), we stress that the square brackets contain the only dependence on θ and ϕ_p. Hence, the polarization dependence of the yield in the jellium models is very simple and the variation with the incident angle is readily calculated once $\epsilon(\omega)$ is prescribed.[37] Experimentally, one has often reported a (near) $\cos^2\phi_p$ dependence of Y,[14,25,28,38] and noted that the yield due to p-polarized light is greatly enhanced at large angles of incidence. Such observations do not prove the validity of a jellium model since various bulk excitation mechanisms can exhibit the same dependencies, but they do support the idea that jellium models successfully describe some of the significant variations. We emphasize that this conclusion is independent of the detailed variation of $V(x)$ and $A_x(x)$ near the surface.

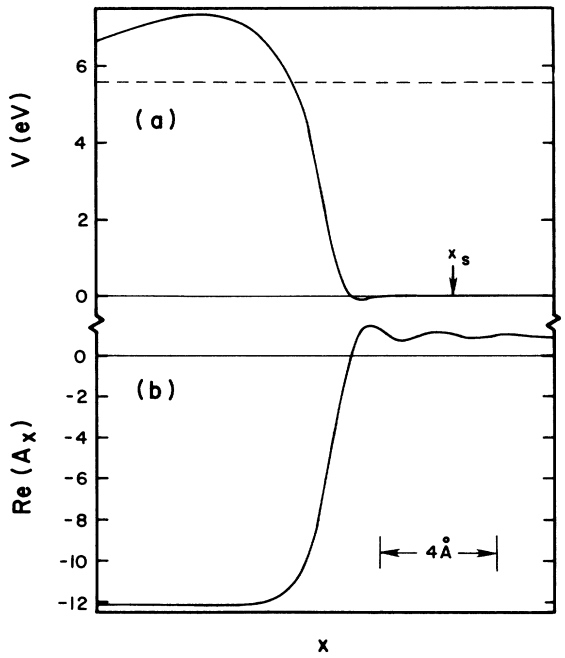

FIG. 1. Typical spatial variations in a jellium model of photofield emission near the surface along the normal coordinate x. In (a) an energy barrier is shown which confines the electrons to the right. On this side V saturates beyond x_s to a constant value, which is taken as the zero of energy. On the left-hand side V has a peak value due to the applied static field. The dashed line denotes the Fermi level. In (b) the real part of the normal component of the vector potential is shown. It has been normalized to go to unity on the right-hand side, while its value on the left differs by a factor of ϵ, the dielectric constant at the excitation frequency. On a wider spatial scale (hundreds of angstroms) A_x will oscillate on the left and decay on the right, but these variations have a negligible effect on the excitation matrix elements.

This region of detailed variation, shown schematically in Fig. 1, is important for determining the magnitude of $Y(E)$ through the matrix element M_{fi}. The terms in front of this in (2) are $f(E-\hbar\omega)$, the Fermi occupation factor for the initial electron state; $W_f(W_i)$, the value of the kinetic energy inside the bulk metal associated with motion along x in the *final* (*initial*) state; and $T(W_f)$, the transmission probability for the photoelectron to escape the metal. This function decreases rapidly with decreasing W_f, if W_f is below the top of the barrier, and serves to cut off the integrals in (1) and (2) before kinematic constraints enter. The matrix element M_{fi} is defined by

$$M_{fi}=\left\langle\phi_f\left|\frac{1}{2}\left[a\frac{d}{dx}+\frac{d}{dx}a\right]\right|\phi_i\right\rangle\,, \tag{5}$$

with a scaled $A_x(x)$ represented by

$$a(x)=\epsilon+(1-\epsilon)\eta(x)\,, \tag{6}$$

where the complex-valued function η varies between 0 and 1 as one goes from just outside to just inside the metal. In Fresnel optics,

$$\eta_F(x)=\Theta(x-x_m)\,, \tag{7}$$

where Θ is the unit step function and x_m locates the plane where one *matches* the vacuum and bulk macroscopic fields. The one-dimensional eigenstates in (5) have also been conveniently scaled. If we denote by x_s the point where $V(x)$ begins its constant bulk value, then

$$\phi_i(x)=\sin(k_i x+\delta_i),\quad x>x_s;\quad W_i=\frac{\hbar^2k_i^2}{2m}\,, \tag{8}$$

$$\phi_f(x)=e^{-ik_f x},\quad x>x_s;\quad W_f=\frac{\hbar^2k_f^2}{2m}=W_i+\hbar\omega\,. \tag{9}$$

The variation of these states in $x<x_s$ depends on the spatial variation of V. Although there is no general analytic solution, one can easily generate them along with $T(W_f)$ and the phase shift δ_i by a numerical solution of Schrödinger's equation.

Our formal description of (2) is now complete, and in the next section we describe its evaluation for various choices of $V(x)$ and $\eta(x)$. For the cases we consider, the magnitude of M_{fi} is most sensitive to the form of the vector potential, as described by $a(x)$. For instance, if one varies the matching plane location in (7) from well inside to well outside the metal (on the scale of Fig. 1), then the effective a acting to photoexcite electrons near the surface changes by a factor of ϵ, so Y changes by $|\,\epsilon\,|^2$. For the model parameters we use,[16] $|\,\epsilon\,|^2\geq 10^2$, so changing x_m by a few angstroms can change Y by several orders of

magnitude. This sensitivity requires careful attention if one hopes to make a quantitative theory of the yield.

MODEL CALCULATIONS

We begin with a description of the various potential-energy barriers that we have used. First, is the step barrier,

$$V_1(x)=V_0\Theta(-x)\ , \tag{10}$$

which crudely represents the system in zero field. The barrier height, $V_0=10.8$ eV,[16] is the sum of the free-electron Fermi energy, $E_F=5.6$ eV, and the work function for W(110), $\Phi=5.2$ eV. The effect of a static field, F, appears in the *triangular barrier* (TB), where

$$V_2(x)=(V_0+eFx)\Theta(-x)\ , \tag{11}$$

where $e>0$. Neither V_1 nor V_2 allow for an image-potential interaction. This feature is included in the image rounded barrier (IRB), for which

$$V_3(x)=\left[V_0+eFx+\frac{e^2}{4x}\right]\Theta(x_s-x)\ . \tag{12}$$

Here, x_s is determined by the condition that V_3 be continuous. Illustrations of V_2 and V_3 are given in Fig. 2 for the choice $F=0.31$ V/Å.[16]

All of the above barriers are models that lack self-consistency. Their shapes are chosen largely for ease of solution and they contain parameters, e.g., V_0, that can be fitted to experimental information that is difficult to calculate. If we require that a barrier be self-consistent, then we must explicitly account for many-electron effects. We do this in one case, but to keep the calculation relatively simple we use a local-density-functional approximation (LDA) to treat the influence of exchange and correlation. The effective one-body potential energy can then be written as

$$V_4(x)=-2\pi e^2\int dx'\,|x-x'|\,[n(x')-n_+(x')]$$
$$+V_{xc}[n(x)]+eFx/2+\bar{V} \tag{13}$$

Here the first term is the (Hartree) potential energy due to the electron density, n, and the ion density, n_+. For a jellium model $n_+(x)=n_B\Theta(x)$, where n_B is the *bulk* density and $x=0$ is at the jellium edge. In the second term we use the approximation proposed by Hedin and Lundqvist.[39] The last two terms are needed to make $V_4\to 0$ as $x\to\infty$ in the presence of an applied field F. The actual values of $V_4(x)$ can only be found numerically as the end result of an iteration procedure which starts from a guess for $V_4(x)$, which allows the calculation of an $n(x)$, which yields a new $V_4(x)$, and so on. Since this procedure has been described in detail elsewhere,[40–42] we only draw in Fig. 2 our final result. For the V_4 shown there, the bulk density is described by the parameter $r_s=3$,[43] and the excess electron density at the surface corresponds to an applied field of

$$4\pi e\int dx\,[n(x)-n_+(x)]=F=0.3\ \text{V/Å}\ . \tag{14}$$

Although V_4 is self-consistent, its neglect of discrete atomic structure leads to a considerable underestimate of the barrier height for W(110) and its use of the LDA makes it lack an $e^2/4x$ term far outside the metal. Hence the IRB is a better choice for comparisons with experiment.

In our basic Eq. (2) the quantity that has the most sensitivity to $V(x)$ is the transmission factor $T(W_f)$. We support this claim in Fig. 3(a) by plotting T versus final energy (normal to the surface) for an electron $\hbar\omega$ above the Fermi level. Since the electron must tunnel for energies less than the barrier maximum, T varies over several orders of magnitude for a modest change in $\hbar\omega$. On the other hand, the scaled matrix element M_{fi} in (2) shows much less change over the same frequency range. This is illustrated in Fig. 3(b). The M_{fi} shown there all use $W_i=E_F$ and $W_f=E_F+\hbar\omega$, and have $a=1$ in Eq. (5) in order to suppress the influence of field variations. As shown in the Appendix, the result for the step barrier is especially simple in this limit [see (A3)] and may be written as

$$M_0(\omega)=(V_0E_F)^{1/2}/\hbar\omega\ . \tag{15}$$

In Fig. 3(b) we normalize the M_{fi} for the other barriers by this expression. The variation of the ratios with $\hbar\omega$ is modest when compared with that of T. This implies that the frequency dependence of the photofield emission yield is essentially determined by that of $|t|^2T(E_F+\hbar\omega)$, although one must know the M_{fi} in order to predict its absolute magnitude.

Since our focus is on the total yield Y, and not its energy distribution $Y(E)$, it is useful to change the order of integration in (1) and (2) to find, in the zero-temperature limit,

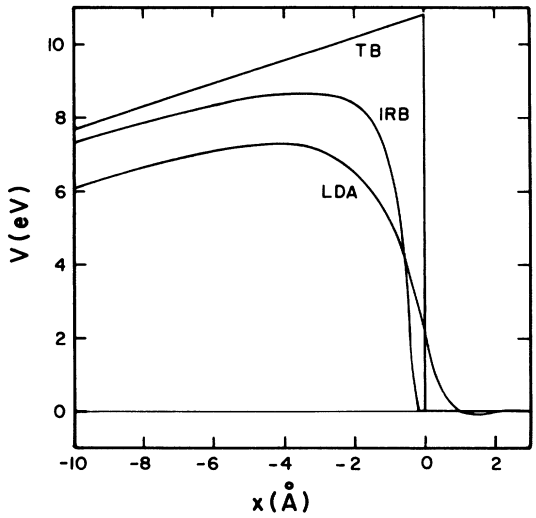

FIG. 2. Various potential-energy barriers vs normal coordinate: TB denotes the triangular barrier, IRB the image-rounded barrier, and LDA the self-consistent barrier found in a local-density-functional approximation. See the text for a further description of their parameters.

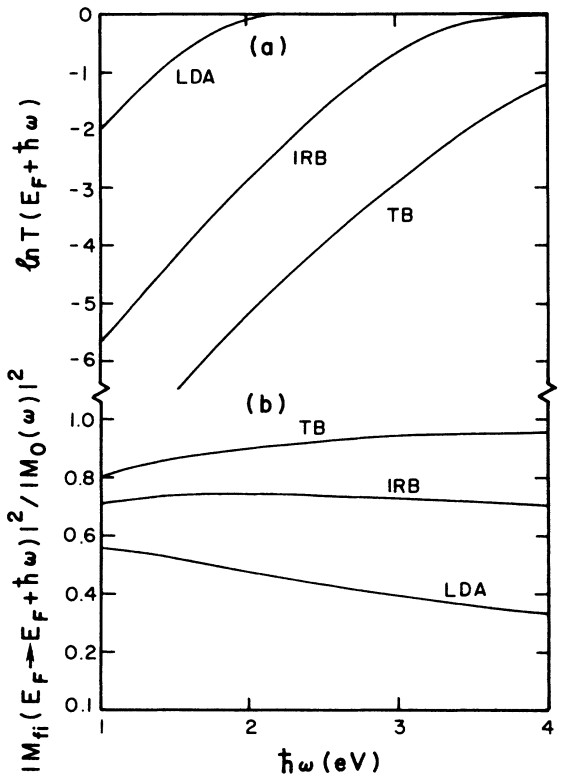

FIG. 3. Photon-frequency dependence of (a) the transmission coefficient for the final-state electron, and (b) the normalized absolute square of the matrix element, ignoring spatial variation of the vector potential. Note the logarithmic scale in (a) and the linear scale in (b). The curve labels refer to the potential-energy barriers shown in Fig. 2. The initial and final states here move only along the surface normal and the initial energy is at the Fermi level E_F.

$$Y=\frac{2\alpha}{\pi}\left[|t|^2\frac{\sin^2\theta}{\cos\theta}\cos^2\phi_p\right]\times\int^{E_F}\frac{dW_i}{(W_iW_f)^{1/2}}\left[\frac{E_f-W_i}{\hbar\omega}\right]T(W_f)|M_{fi}|^2 . \tag{16}$$

Thus only one integral needs to be done numerically and the range of W_i in (16) is from E_F down to where $T(W_i+\hbar\omega)$ becomes negligible.

To calculate the M_{fi} we need both $V(x)$, which determines the initial and final eigenstates, and $\eta(x)$, which describes the spatial variation of the perturbing field. A common approximation in photoemission theory is to completely ignore the latter variation by setting $\eta\equiv 1$. In previous photofield emission theories the only explicit improvement on this has been by the use of the η that results from Fresnel optics, see Eq. (7).[8,16,44] This contains as a free parameter x_m, the position of the matching plane. We reconsider here the predictions of these η's, but also illustrate the effect of several further refinements.

The improvements come specifically from the calculational scheme developed by Kempa and Schaich,[45–47] which represents one of several approaches that have recently appeared.[48,49] The simplest improvement over the Fresnel approximation is called the ansatz[46] and determines η from the equilibrium electron-density profile:

$$\eta_A(x)=n_0(x)/n_B , \tag{17}$$

where

$$n_0(x)=3n_B\int_0^1 d(k_i/k_F)[1-(k_i/k_F)^2]\phi_i^2(x) . \tag{18}$$

Here, k_F is the Fermi wave vector and the occupied eigenstates are normalized as in (8) so $n_0(x\to\infty)\to n_B$. This approximation to η smoothes out the discontinuity in η_F and removes the free parameter x_m. However, it is not frequency dependent, nor is it exact at any frequency, although it agrees reasonably well with detailed jellium model calculations[46] at frequencies below the plasmon frequency, ω_p.[43]

To remove these deficiencies requires considerable computational effort. We examine here two further cases. The first we call $\eta_0(x)$, since it comes from a full calculation at $\omega=0$, but we shall use it without modification over the whole photofield-emission frequency range. To estimate the size of error this entails, we also calculate η at one finite frequency, $\omega/\omega_p=0.25$. The analysis behind these last two η's has been amply described elsewhere.[45–47] We only note here that they both represent a random-phase approximation to the linear

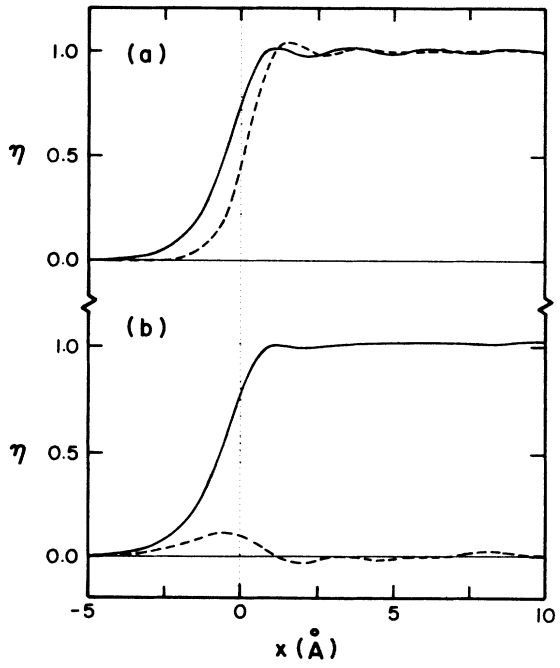

FIG. 4. Normalized plots of the field variation near the surface of a LDA model, whose potential-energy barrier is shown in Fig. 2. The function η is defined by Eqs. (5) and (6). In (a) the solid curve gives η calculated from the system response at zero excitation frequency, while the dashed curve is η found from the ansatz (17). In (b) the real (imaginary) part of η is shown by the solid (dashed) curve calculated at the excitation frequency $\omega/\omega_p=0.25$.

response of a system whose ground state is described by the LDA.

In Fig. 4 we compare these various η's, as calculated for the LDA barrier shown in Fig. 2. Notice their similar shapes but relative shifts along the surface normal. An analogue of the matching plane position x_m of the Fresnel η_F can be defined as

$$d_\perp = \int dx\,[\Theta(x)-\eta(x)] = \int dx\, x\frac{d\eta}{dx}\ , \tag{19}$$

where we have used the notation of Feibelman[50] for the d parameter. For η_F and η_A (of LDA model) the integral is easy,

$$d_\perp^A = -\frac{F}{4\pi n_B e}\ , \tag{21}$$

and the value of $d_\perp^A$ for $r_s=3$ and $F=0.3$ V/Å is -0.028 Å. For the η's coming from the full calculation, we can only list the numerical values

$$d_\perp(\omega=0) = -0.67 \text{ Å}\ , \tag{22}$$

$$d_\perp(\omega=0.25\omega_p) = (-0.79-i0.24) \text{ Å}\ . \tag{23}$$

The relative order of these $d_\perp$'s agrees with the alignment of the η's in Fig. 4. Note the relatively small change (at least in the real part) of the results for $\omega=0$ and $\omega/\omega_p=0.25$.

Before describing our model calculations for Y, we remark that we evaluate the matrix elements M_{fi} by using (5) directly. If a (i.e., η) is independent of position, the matrix element can be exactly rewritten as proportional to a matrix element of dV/dx, which for a steplike V is easily evaluated. When a is position dependent, this transformation based on a commutator identity can still be done, as we show in the Appendix, but it provides no particular simplification. Hence we do not use this transformation in our calculations, although Gao and Reifenberger did in theirs.[16] The important point is that the transformation, if done correctly, is exact.[51]

We have now described various approximations for the different ingredients that must be combined to give Y in (16). If one is aiming to compare directly with experimental data,[16] then any jellium model will be quite inadequate unless it incorporates some parameters that can be adjusted in order to mimic the effects of discrete lattice structure. We make the following changes from a pure jellium model, such as one based on the LDA and the η's in Fig. 4. The values of the dielectric function needed to evaluate t in (3) are taken from an experimental compilation.[52] For $V(x)$ we use the IRB shown in Fig. 2, whose height has been adjusted to agree with other experiments.[53] To retain the freedom of a fitting parameter, we calculate Y using the Fresnel η_F for several choices of x_m, measured from the coordinate zero in Fig. 2. Typical results are shown in Fig. 5 along with experimental data points.[54] At any ω, the yield appears to be a monotonically increasing function of x_m, which is easy to understand from (6) and the large magnitude of $\epsilon(\omega)$. To fit the data would require $x_m \simeq -2$ Å at low frequency, and a slightly more negative x_m at larger ω. As we discuss below, these values are not unreasonable. In an analogous Fresnel-IRB calculation for W(111), where $V_0=10.0$ eV, the x_m that fit the data[16] are about -1.5 Å.

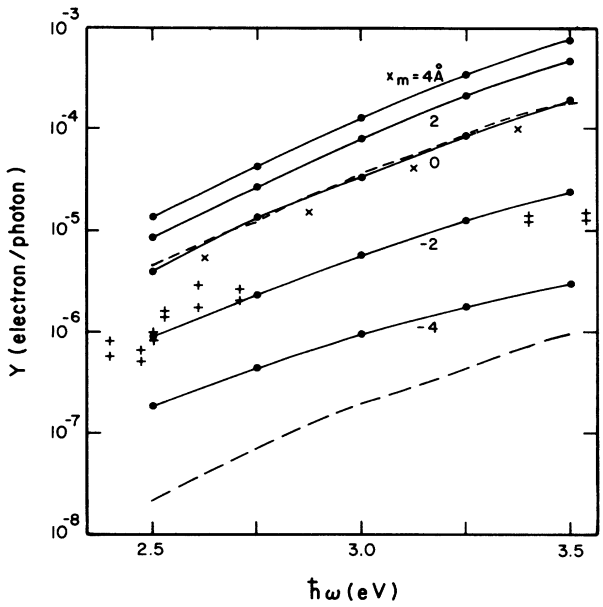

FIG. 5. Photon-frequency dependence of the yield in electrons per incident photon at 70°. The image-rounded barrier is used for $V(x)$ and experimental values for the dielectric function $\epsilon(\omega)$. The various sets of solid points (connected by lines for clarity) are found from the Fresnel model of field variation. The matching plane location labels each set. The dashed curves result from the approximate, analytic matrix elements found in the Appendix. The lower one is from (A3) and the higher one is from (A7). The predictions of the ansatz model of field variation are denoted by $\times$'s. Finally the data from Ref. 16 for W(110) have been scaled to our units and plotted as $+$'s.

We also show in Fig. 5 other approximate results. The dashed curves come from using different $V(x)$'s in the calculations of $T(W_f)$ and M_{fi}; specifically, the IRB is used for $T(W_f)$ and the step barrier is used to evaluate M_{fi}. Such a inconsistent approach has been used before,[3,16] but from Fig. 3 we expect it to differ only slightly from a full IRB evaluation. The upper dashed curve uses η_F with $x_m=0$ and essentially agrees with the full IRB result. The lower dashed curve uses $\eta\equiv 1$. This curve can also be thought as coming from any η_F with $x_m<-10$ Å. The simple form of V and η_F for the dashed curves allow one to find analytic expressions for their M_{fi}, which are derived in the Appendix.

The remaining x's plotted in Fig. 5 result from the IRB model together with its ansatz η_A. For the IRB shown in Fig. 2, $d_\perp^A(\text{IRB})=-0.358$ Å. Indeed, the results for Y are quite similar to what one gets if η_F with $x_m=d_\perp^A(\text{IRB})$ is used instead. The implication is that for the frequencies considered here the detailed shape of η is not as important as is the value of the real part of $d_\perp$.

We can further explore the validity of this idea by cal-

culations with the LDA barrier. Since we want to treat both V and η in the same way, we switch to a pure jellium-model calculation. Thus we now use the real valued Drude $\epsilon(\omega)=1-\omega_p^2/\omega^2$ and find $T(W_f)$ from the LDA barrier, both for $r_s=3$.[43] There are no free parameters and a comparison with tungsten data would be poor. However, our present aim is only to exhibit the effect of different approximations for η, specifically those curves shown in Fig. 4. The results are plotted in Fig. 6. Using either η_A or η_F with the same $d_\perp$ gives essentially the same results. Switching to η_0, whose $d_\perp$ according to (22) is slightly farther out in vacuum, gives a slightly smaller yield. The approximation of using η_0 for all the frequencies in the plot is not severe since correcting it at $\omega/\omega_p=0.25$, where it should be worse, it virtually unnoticeable. This is somewhat surprising considering the difference between η's shown in Fig. 4, but not unimaginable. In a similar sense we can claim that the size of x_m needed in Fig. 5 to fit the W(110) data is reasonably close to the $d_\perp$'s of Eqs. (22) and (23).

We conclude that the predictions of a pure jellium model are fairly certain, since all the points at any ω in Fig. 6 are close. However, such models cannot represent transition metals. When one adapts the jellium model to tungsten by introducing parameters fitted to experiment, i.e., $\epsilon(\omega)$, V_0 in an IRB, and x_m in η_F, then reasonable choices do allow good agreement with experiment. For future work, we note that while considerable effort has been made to incorporate band-structure effects into the calculation both of $\epsilon(\omega)$ and of the surface potential-energy–barrier shape, only qualitative discussions have been made about their influence on η. It is in this latter area that we are presently developing quantitative methods.

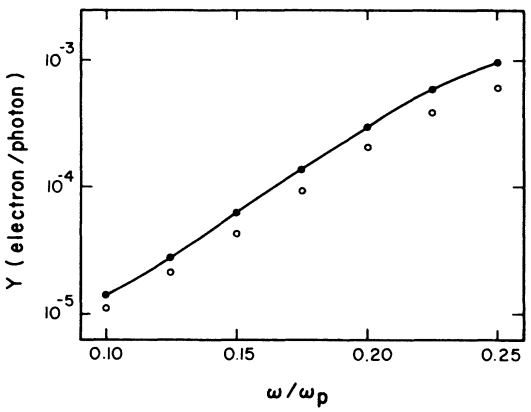

FIG. 6. Photon-frequency dependence of the yield in electrons per incident photon at 70°. The LDA barrier shown in Fig. 2 is used for $V(x)$ and the dielectric function is $\epsilon(\omega)=1-\omega_p^2/\omega^2$. The solid points (connected by lines to guide the eye) are found from the Fresnel model of field variation. The matching plane location is at $d_\perp^A$ of (21). The Fresnel results agree to within the size of the points with those calculated from the ansatz field, shown in Fig. 4(a). The open circles are found by using the η function calculated at $\omega=0$ [also shown in Fig. 4(a)] for all frequencies. The results from the η function shown in Fig. 4(b), evaluated at $\omega/\omega_p=0.25$, lies within the open circle plotted here at that frequency.

ACKNOWLEDGMENTS

We wish to thank Dr. A. Liebsch and Dr. L. Lou for help in setting up the LDA barrier calculations and Dr. Y. Gao and Dr. R. Reifenberger for clarifying discussions. The full calculations of η were done on the Cray 48X-MP computer run by the National Center for Supercomputing Applications at the University of Illinois. Our time allowance there, as well as other partial support, was provided by the National Science Foundation through Grant No. DMR-85-12709.

APPENDIX

Here we develop an alternate expression for the matrix element M_{fi} in (5) and make contact with the estimate of Gao and Reifenberger,[16] called GR here. We begin by setting $h_1=\frac{1}{2}[a(d/dx)+(d/dx)a]$ and applying the commutator identity

$$\hbar\omega M_{fi}=\langle\phi_f|[h_0,h_1]|\phi_i\rangle\ , \tag{A1}$$

where $h_0=p^2/2m+V(x)$; $p=\hbar d/i\,dx$ is the (one-dimensional) unperturbed Hamiltonian. Both ϕ_i and ϕ_f are eigenfunctions of h_0, whose eigenvalues differ by $\hbar\omega$.

Explicitly working out the commutator gives

$$\hbar\omega M_{fi}=\langle\phi_f|-a\left[\frac{dV}{dx}\right]+\frac{1}{2m}\left[\frac{p^2}{2}\left[\frac{da}{dx}\right]+p\left[\frac{da}{dx}\right]p+\left[\frac{da}{dx}\right]\frac{p^2}{2}\right]|\phi_i\rangle\ . \tag{A2}$$

A common approximation in photoemission theory ignores the spatial variation of a, replacing it by its unit value inside the metal. If furthermore V has a step function form $V(x)=V_0\Theta(-x)$, then

$$M_{fi}\simeq\frac{V_0}{\hbar\omega}\phi_f^*(0)\phi_i(0)=\frac{V_0}{\hbar\omega}\left[\frac{W_i}{V_0}\right]^{1/2}\ , \tag{A3}$$

where the second expression follows from $\phi_i(0)=\sin\delta_i=(W_i/V_0)^{1/2}$. This result is equivalent to GR's simplest estimate. Note that for photofield emission it not only approximates a, but also neglects the effect of the applied static field on M_{fi}.[7]

An improvement of (A3) can be made by allowing a to have the Fresnel form, as described in (6) and (7). Then both dV/dx and da/dx are proportional to δ functions, so the integral in (A2) can still be explicitly done. However, some mathematical care is necessary if x_m in (7) vanishes, i.e., if the radiation field and the potential energy have discontinuities at the same point. This leads, in (A2), to expressions proportional to $\Theta(x)\delta(x)$, where $\delta(x)=(d/dx)\Theta(x)$ is a δ function. We interpret such products as

$$\Theta(x)\delta(x)=\frac{1}{2}\frac{d}{dx}[\Theta(x)\Theta(x)]$$

$$=\frac{1}{2}\frac{d}{dx}\Theta(x)=\tfrac{1}{2}\delta(x)\ . \tag{A4}$$

Hence, for smooth "test functions," $b_1(x)$ and $b_2(x)$, we find for $B(x)=b_1(x)+\Theta(x)b_2(x)$ that the integral across $x=0$ is

$$\int dx\ \delta(x)B(x)=b_1(0)+\tfrac{1}{2}b_2(0)$$

$$=\tfrac{1}{2}[B(0^+)+B(0^-)]\ , \tag{A5}$$

where 0^+ (0^-) is just above (below) 0. GR use an alternate, physical reduction of (A5); however, our scheme makes M_{fi} a continuous function of x_m, while theirs does not.

Using (A5) in (A2) for a model with a single-step discontinuity at $x=0$ in both V and a yields

$$\hbar\omega M_{fi}=\left\{V_0\left[\frac{1+\epsilon}{2}\right]+(1-\epsilon)\frac{1}{2}\left[\left[W_f-\frac{V_0}{2}\right]+\left[W_i-\frac{V_0}{2}\right]\right]\right\}\phi_f^*(0)\phi_i(0)+(1-\epsilon)\frac{\hbar^2}{2m}\frac{d\phi_f^*}{dx}(0)\frac{d\phi_i}{dx}(0)\ . \tag{A6}$$

From the solutions of Schrödinger's equation for a single step barrier one can reduce (A6) to

$$\hbar\omega M_{fi}=\left[\frac{W_i}{V_0}\right]^{1/2}\left[V_0\left[\frac{1+\epsilon}{2}\right]+(1-\epsilon)\left[\frac{\hbar\omega}{2}+W_i-\frac{V_0}{2}+i(W_f(V_0-W_i))^{1/2}\right]\right]\ , \tag{A7}$$

which is similar to, but different from, GR's result that "allows for spatial variation in **A**." The predictions from both (A3) and (A7) have been plotted in Fig. 5.

[1]H. Neumann, Physica **44**, 587 (1969).
[2]B. I. Lundqvist, K. Mountfield, and J. W. Wilkins, Solid State Commun. **10**, 383 (1972).
[3]A. Bagchi, Phys. Rev. B **10**, 542 (1974).
[4]C. Caroli, D. Lederer-Rozenblatt, B. Roulet, and D. Saint-James, Phys. Rev. B **10**, 861 (1974).
[5]E. Taranko, Acta Phys. Pol. A **49**, 721 (1976).
[6]E. Taranko, Acta Phys. Pol. A **53**, 761 (1978).
[7]C. Schwartz and M. W. Cole, Surf. Sci. **95**, L243 (1980).
[8]C. Schwartz and W. L. Schaich, Phys. Rev. B **24**, 1583 (1981).
[9]C. Schwartz and M. W. Cole, Surf. Sci. **115**, 290 (1982).
[10]R. Reifenberger, D. L. Haavig, and C. M. Egert, Surf. Sci. **109**, 276 (1981).
[11]R. A. Young, Solid State Commun. **45**, 263 (1983).
[12]A. Puri and W. L. Schaich, Phys. Rev. B **28**, 1781 (1983).
[13]J.-W. Wu and G. D. Mahan, Phys. Rev. B **28**, 4839 (1983).
[14]D. Venus and M. J. G. Lee, Surf. Sci. **125**, 452 (1983).
[15]D. L. Haavig and R. Reifenberger, Surf. Sci. **151**, 128 (1985).
[16]Y. Gao and R. Reifenberger, Phys. Rev. B **35**, 8301 (1987).
[17]H. Neumann and Ch. Kleint, Ann. Phys. (Leipzig) **27**, 237 (1971).
[18]T. Radon and Ch. Kleint, Surf. Sci. **60**, 540 (1976).
[19]E. Taranko, J. Phys. (Paris) **38**, 163 (1977).
[20]Ch. Kleint and T. Radon, Surf. Sci. **70**, 131 (1978).
[21]T. Radon, Surf. Sci. **100**, 353 (1980).
[22]D. Venus and M. J. G. Lee, Phys. Rev. B **28**, 437 (1983).
[23]T. Radon and Ch. Kleint, Surf. Sci. **144**, 638 (1984).
[24]A. Modinos and Ch. Kleint, Solid State Commun. **50**, 651 (1984).
[25]Y. Gao and R. Reifenberger, Phys. Rev. B **32**, 1380 (1985).
[26]D. Venus and M. J. G. Lee, Surf. Sci. **172**, 477 (1986).
[27]D. Venus and M. J. G. Lee, Phys. Rev. B **34**, 4449 (1986).
[28]Y. Gao and R. Reifenberger, Phys. Rev. B **35**, 4284 (1987).
[29]Y. Gao and R. Reifenberger, Phys. Rev. B **35**, 6627 (1987).
[30]M. J. G. Lee, Phys. Rev. Lett. **30**, 1193 (1973).
[31]R. Reifenberger, H. A. Goldberg, and M. J. G. Lee, Surf. Sci. **83**, 599 (1979).
[32]D. L. Haavig and R. Reifenberger, Surf. Sci. **151**, 128 (1985).
[33]P. J. Feibelman, Phys. Rev. Lett. **34**, 1092 (1975).
[34]P. J. Donders and M. J. G. Lee, Surf. Sci. **160**, 280 (1985).
[35]W. L. Schaich, in *Many-Body Phenomena at Surfaces,* edited by D. Langreth and H. Suhl (Academic, New York, 1984).
[36]W. L. Schaich, in *Photoemission in Solids,* edited by M. Cardona and L. Ley (Springer, New York, 1978), Vol. 1.
[37]P. J. Feibelman, Surf. Sci. **46**, 558 (1974).
[38]Y. Teisseyre, R. Haug, and R. Coelho, Surf. Sci. **87**, 549 (1979).
[39]L. Hedin and B. I. Lundqvist, J. Phys. C **4**, 2064 (1971).
[40]A. Liebsch, J. Phys. C **19**, 5025 (1986).
[41]P. Gies and R. R. Gerhardts, Phys. Rev. B **33**, 982 (1986).
[42]F. Schreir and F. Rebentrost, J. Phys. C **20**, 2609 (1987).
[43]For $r_s=3$, $E_F=5.57$ eV and $\hbar\omega_p=9.07$ eV.
[44]C. M. Egert and R. Reifenberger, Surf. Sci. **145**, 159 (1984).
[45]K. Kempa and W. L. Schaich, Phys. Rev. B **34**, 547 (1986).
[46]W. L. Schaich, and K. Kempa, Phys. Scr. **35**, 204 (1987).
[47]K. Kempa and W. L. Schaich, Phys. Rev. B **37**, 6711 (1988).
[48]P. Gies, R. R. Gerhardts, and T. Maniv, Phys. Rev. B **35**, 458 (1987).
[49]A. Liebsch, Phys. Rev. B **36**, 7378 (1987).
[50]P. J. Feibelman, Prog. Surf. Sci. **12**, 287 (1982).
[51]We disagree with the claim by B. C. Meyers and T. E. Feuchtwang [Phys. Rev. B **27**, 2030 (1983)] that "the matrix element for photoexcitation can be evaluated directly and . . . it differs from the transformed matrix element."
[52]*Handbook of Optical Constants of Solids,* edited by E. D. Palik (Academic, Orlando, 1985).
[53]T. V. Vorburger, D. Penn, and E. W. Plummer, Surf. Sci. **48**, 417 (1978).
[54]The specific algorithm one should use to convert the relative yield, Y_R, of Ref. 16 to our absolute yield, Y, is $Y=(Y_R/\cos\theta)J_T/F_p$, where $J_T=197$ electrons/Å^2 s is the theoretical tunneling current at 300 K and $F_p=199$ photons/Å^2 s is the characteristic photon flux [Y. Gao and R. Reifenberger (private communication)].